

**New fit to the reaction  $\gamma p \rightarrow K^+ \Sigma^0$** 

Oren V. Maxwell

*Department of Physics, Florida International University, University Park, Miami, Florida 33199, USA*

(Received 25 June 2015; published 26 October 2015)

The reaction  $\gamma p \rightarrow K^+ \Sigma^0$  has been investigated using a tree-level effective Lagrangian model similar to that employed previously by the author to study the electromagnetic production of  $\Lambda$ 's from protons. In addition to the Born terms, the model incorporates a number of baryon resonances with spins up to  $\frac{5}{2}$  and the two kaon resonances,  $K^*(892)$  and  $K_1(1270)$ . Momentum- and energy-dependent widths for the nucleon and  $\Delta$  resonances are included by means of a dynamical model that makes use of empirical on-shell branching ratios. The model parameters, consisting of products of the coupling strengths at the electromagnetic and strong interaction vertices in the resonance contributions, are fit to a large pool of photoproduction data from the CLAS and GRAAL Collaborations. Results are presented for the unpolarized differential cross section, the photon beam asymmetry  $\Sigma$ , the hyperon recoil asymmetry  $P$ , and the double-polarization observables  $C_x$  and  $C_z$  in a variety of kinematical situations and compared with the data.

DOI: [10.1103/PhysRevC.92.044614](https://doi.org/10.1103/PhysRevC.92.044614)

PACS number(s): 24.10.Jv, 25.10.+s, 25.20.Lj, 13.60.-r

**I. INTRODUCTION**

The electromagnetic production of strangeness from protons and other light nuclei has been a major field of interest within the nuclear physics community for well over 2 decades. The extra degree of freedom represented by the strange quark makes the investigation of reactions involving strange baryons imperative for gaining a fuller understanding of the strong interaction within a nuclear environment. Most of the effort in strangeness photoproduction studies has focused on the  $K^+ \Lambda$  reaction channel, because the relatively long life of the  $\Lambda$  combined with the nonzero charge of the  $K^+$  makes this channel the easiest to study experimentally. However, a number of recent measurements of the  $\gamma p \rightarrow K^+ \Lambda$  reaction have also included data for the  $\gamma p \rightarrow K^+ \Sigma^0$  reaction, and the data obtained for the latter reaction are copious enough and of sufficient quality to warrant a separate theoretical examination of that reaction.

Theoretical studies of strangeness photoproduction from the proton date back to the late 1960s and early 1970s [1,2], but the theoretical work at that time was severely hampered by the lack of empirical data. There was renewed interest in the field beginning in the late 1980s [3–12] when better quality data started to become available, but, as mentioned above, this work focused mainly on  $\Lambda$  production. Theoretical studies that include  $\Sigma^0$  production are of more recent vintage and much fewer in number [13–18].

The work reported here is based on a model developed earlier for the analysis of the  $\gamma p \rightarrow K^+ \Lambda$  reaction [19]. An earlier version of the model was used to study the photoproduction of  $\Lambda$ 's from the deuteron and  $^3\text{He}$  [11,20,21], and an extension of the model with electromagnetic form factors incorporated was employed in studies of  $\Lambda$  electroproduction from the proton and the deuteron [22,23]. The model is a tree-level effective Lagrangian model consisting of  $s$ -channel,  $u$ -channel, and  $t$ -channel contributions. The main difference between  $\Lambda$  production and  $\Sigma^0$  production in such a model is that the isospin of the  $\Sigma$  permits  $\Delta$  resonance intermediate states to be excited. Aside from the inclusion of  $\Delta$  resonances, the model described here differs from the earlier model in

the incorporation of data from a more recent version of the particle data tables [24] and in some adjustments to the set of nucleon resonances that are included in the  $s$  channel. Details are presented in Sec. II.

The fitting procedure is described in Sec. III. The parameters of the model were fit to CLAS data for the unpolarized differential cross section [25,26], the hyperon recoil asymmetry [26,27], and a pair of double-polarization observables [28], as well as GRAAL data for the photon beam asymmetry [29]. The model parameters determined in the fit, consisting of products of the coupling strengths at the electromagnetic and strong interaction vertices in the resonance contributions, are listed in Sec. IV. Section IV also contains a discussion of the results, some conclusions, and a brief outline of future work.

**II. REACTION MODEL**

The reaction model is based on three types of contributions, depicted in Fig. 1, which are designated  $s$ -channel,  $u$ -channel, or  $t$ -channel contributions according to whether the squared four-momentum in the intermediate state propagator corresponds to the  $s$ ,  $t$ , or  $u$  Mandelstaam variable. In each channel, the Born terms are supplemented with terms involving the excitation of intermediate hadronic resonances appropriate to that channel.

Table I lists all of the baryon resonances that have been incorporated in the model. In the  $s$ -channel, these include all of the well-established nucleon and  $\Delta$  resonances (three- and four-star status) with spins less than or equal to  $\frac{5}{2}$  that appear in the most recent particle data tables [24]. I have also incorporated a number of two-star resonances of higher energy, including  $N(1860)$ ,  $N(1880)$ , and  $N(2000)$ . Inclusion of these higher energy resonances improves the data fits at the higher energy end. A number of other two-star nucleon and  $\Delta$  resonances, such as  $N(1895)$ ,  $N(2060)$ ,  $N(2120)$ ,  $\Delta(1900)$ ,  $\Delta(1940)$ , and  $\Delta(2000)$ , have been excluded because there is no evidence for these resonances in the most recent George Washington University analysis, despite their two-star status in the particle data tables. I have also excluded two other nucleon

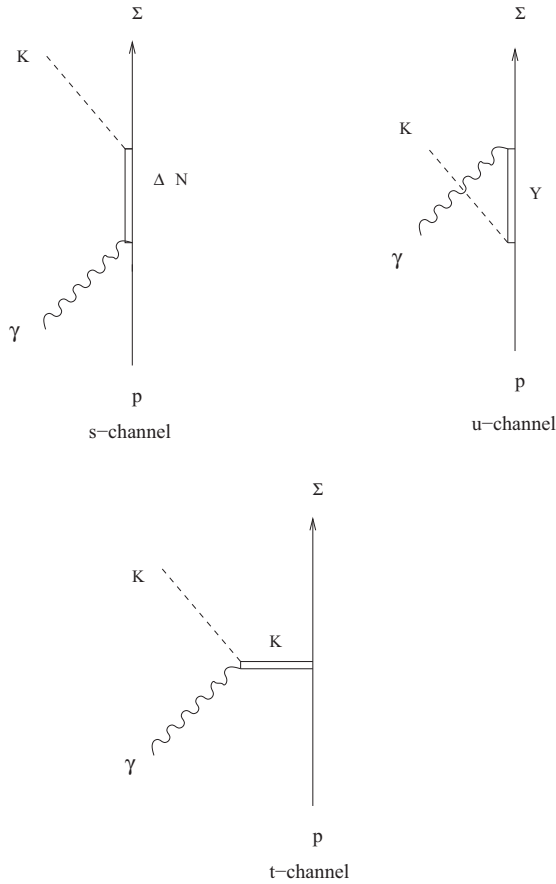


FIG. 1. Contributions to the amplitude for the reaction  $\gamma p \rightarrow K^+ \Sigma^0$ .

resonances, the spin  $\frac{3}{2}$   $N(2080)$  and the spin  $\frac{5}{2}$   $N(2200)$ , that were included in earlier fits to  $\Lambda$  production data [19,22], but which have since disappeared from the particle data tables.

In the  $u$  channel, the resonances incorporated are the same as those incorporated in the earlier fits to  $\Lambda$  production data [19,22]. In Ref. [19], it was shown that the inclusion of more resonances in the  $u$  channel does not materially improve the fits. I have also employed the same  $t$ -channel kaon resonances that were incorporated in the earlier  $\Lambda$  production fits, namely, the  $K^*(892)$  and  $K_1(1270)$  resonances. These two kaon resonances have been included in almost all of the more recent analyses of photoproduction data that are based on an effective Lagrangian model.

The  $s$ -,  $u$ -, and  $t$ -channel contributions to the reaction amplitude in the impulse approximation have the general forms

$$\hat{T}_s = \sum_{N, \Delta} \mathcal{V}_K^\dagger(p_K) D(p_s) \mathcal{V}_\gamma(p_\gamma), \quad (1)$$

$$\hat{T}_u = \sum_Y \mathcal{V}_\gamma^\dagger(p_\gamma) D(p_u) \mathcal{V}_K(p_K), \quad (2)$$

and

$$\hat{T}_t = \sum_K \mathcal{V}_{\gamma K}^\dagger(p_\gamma, p_t) D_t(p_t) \mathcal{V}_{p\Sigma}(p_t), \quad (3)$$

TABLE I. Baryon resonances considered in the model.

Resonance	$J^P$
$N(1440)$	$\frac{1}{2}^+$
$N(1520)$	$\frac{3}{2}^-$
$N(1535)$	$\frac{1}{2}^-$
$N(1650)$	$\frac{1}{2}^-$
$N(1675)$	$\frac{3}{2}^-$
$N(1680)$	$\frac{3}{2}^+$
$N(1700)$	$\frac{3}{2}^-$
$N(1710)$	$\frac{1}{2}^+$
$N(1720)$	$\frac{3}{2}^+$
$N(1860)$	$\frac{3}{2}^+$
$N(1875)$	$\frac{3}{2}^-$
$N(1880)$	$\frac{1}{2}^+$
$N(1900)$	$\frac{3}{2}^+$
$N(2000)$	$\frac{3}{2}^+$
$\Delta(1232)$	$\frac{3}{2}^+$
$\Delta(1600)$	$\frac{3}{2}^+$
$\Delta(1620)$	$\frac{1}{2}^-$
$\Delta(1700)$	$\frac{3}{2}^-$
$\Delta(1905)$	$\frac{3}{2}^+$
$\Delta(1910)$	$\frac{1}{2}^+$
$\Delta(1920)$	$\frac{3}{2}^+$
$\Delta(1930)$	$\frac{3}{2}^-$
$\Lambda(1405)$	$\frac{1}{2}^-$
$\Lambda(1670)$	$\frac{1}{2}^-$
$\Lambda(1820)$	$\frac{3}{2}^+$
$\Lambda(1830)$	$\frac{3}{2}^-$
$\Lambda(1890)$	$\frac{3}{2}^+$
$\Lambda(2110)$	$\frac{3}{2}^+$
$\Sigma(1385)$	$\frac{3}{2}^+$
$\Sigma(1775)$	$\frac{3}{2}^-$
$\Sigma(1915)$	$\frac{3}{2}^+$
$\Sigma(1940)$	$\frac{3}{2}^-$

where  $p_s = p_\Sigma + p_K$ ,  $p_u = p_\Sigma - p_\gamma$ , and  $p_t = p_\gamma - p_K$  are the intermediate four-momenta in the  $s$ -,  $u$ -, and  $t$ -channel amplitudes, respectively. The  $\mathcal{V}$ 's here are the vertex functions at the electromagnetic and strong interaction vertices, and the  $D$ 's are the intermediate hadron propagators. Note that the sums include the Born terms as well as the resonance contributions.

The vertex functions and propagators in these expressions depend upon the spins and parities of the intermediate resonances. The various forms adopted here are the same as those employed in the earlier  $\Lambda$  production fits and are discussed in detail in Ref. [19]. Here I just summarize the forms employed.

In the  $t$  channel, the vertex functions are given by

$$\mathcal{V}_{\gamma K} = e\epsilon(2p_K - p_\gamma) \quad (4)$$

and

$$\mathcal{V}_{p\Sigma} = g_{\Sigma K p}\gamma_5 \quad (5)$$

for an intermediate ground-state kaon (the  $t$ -channel Born term), by

$$\mathcal{V}_{\gamma K}^\mu = \frac{g_{\gamma K K^*}}{m_{sc}} \epsilon^{\mu\nu\rho\lambda} \epsilon_\nu p_{\gamma\rho} p_{t\lambda} \quad (6)$$

and

$$\mathcal{V}_{p\Sigma}^\mu = \left( g_{\Sigma K^* p}^V + \frac{g_{\Sigma K^* p}^T}{m_p + m_\Sigma} \gamma p_t \right) \gamma^\mu \quad (7)$$

for an intermediate  $K^*(892)$  resonance, and by

$$\mathcal{V}_{\gamma K}^\mu = \frac{g_{\gamma K K^* 1}}{m_{sc}} (\epsilon p_t p_\gamma^\mu - p_\gamma p_t \epsilon^\mu) \quad (8)$$

and

$$\mathcal{V}_{p\Sigma}^\mu = \left( g_{\Sigma K^* 1 p}^V + \frac{g_{\Sigma K^* 1 p}^T}{m_p + m_\Sigma} \gamma p_t \right) \gamma^\mu \gamma_5 \quad (9)$$

for an intermediate  $K^*(1270)$  resonance, where  $\epsilon$  is the photon polarization four-vector and  $m_{sc}$  is a scaling mass that has been set equal to 1000 MeV. Because the kinematics of the photoproduction reaction preclude intermediate resonance decay in the  $t$  channel, the kaon resonance propagator does not include a width. Thus,

$$D_t = \frac{-g_{\mu\nu} + \frac{p_{t\mu} p_{t\nu}}{m_{K^*}^2}}{p_t^2 - m_{K^*}^2}. \quad (10)$$

In the  $s$  and  $u$  channels, the vertex functions are given by

$$\mathcal{V}_{K\frac{1}{2}^+}(p_K) = g\gamma_5 \quad (11)$$

and

$$\mathcal{V}_{\gamma\frac{1}{2}^+}(p_\gamma) = g_\gamma \epsilon_\mu i\sigma^{\mu\nu} (p_\gamma)_\nu, \quad (12)$$

with

$$g_\gamma = \frac{e\kappa}{2m_B}, \quad (13)$$

for positive parity intermediate baryons of spin  $\frac{1}{2}$ . The negative parity vertex functions are just the positive parity functions with the  $\gamma_5$  factor moved from the strong interaction vertex to the electromagnetic vertex. Here  $m_B$  is equal to the proton mass in the  $s$  channel and to the  $\Sigma$  mass in the  $u$  channel. The  $s$ -channel Born contribution has an additional charge term,

$$\mathcal{V}_{\text{charge}}(p_\gamma) = e\gamma^\mu \epsilon_\mu, \quad (14)$$

that has to be added to the electromagnetic vertex given above.

For positive parity intermediate resonances of higher spin, the vertex functions are

$$\mathcal{V}_{K\frac{3}{2}^+}(p_K) = -\frac{g}{m_\pi} p_K^\mu, \quad (15)$$

$$\mathcal{V}_{K\frac{5}{2}^+}(p_K) = \frac{g}{m_\pi^2} p_K^\mu p_K^\nu \gamma_5, \quad (16)$$

$$\mathcal{V}_{\gamma\frac{3}{2}^+}(p_\gamma) = \left[ \frac{g_1}{2m_B} (\epsilon^\mu \gamma p_\gamma - p_\gamma^\mu \gamma \epsilon) + \frac{g_2}{4m_B^2} (\epsilon p_B p_\gamma^\mu - p_\gamma p_B \epsilon^\mu) \right] \gamma_5, \quad (17)$$

and

$$\mathcal{V}_{\gamma\frac{5}{2}^+}(p_\gamma) = \left[ \frac{g_1}{2m_B} (\epsilon^\mu \gamma p_\gamma - p_\gamma^\mu \gamma \epsilon) + \frac{g_2}{4m_B^2} (\epsilon p_B p_\gamma^\mu - p_\gamma p_B \epsilon^\mu) \right] \frac{p_\gamma^\nu}{m_\pi}, \quad (18)$$

where  $p_B$  is the ground-state baryon four-momentum and the factor  $m_\pi$  has been introduced to make  $g$  dimensionless. The corresponding propagators are constructed by multiplying the Dirac propagator,

$$D^{\frac{1}{2}}(p) = \frac{\gamma p + m_I}{p^2 - m_I^2 + im_I \Gamma_I}, \quad (19)$$

on the right by either the spin  $\frac{3}{2}$  projection operator,

$$P_{\mu\nu}^{\frac{3}{2}} = g_{\mu\nu} - \frac{1}{3} \gamma_\mu \gamma_\nu + \frac{1}{3} \frac{p_\mu \gamma_\nu - p_\nu \gamma_\mu}{m_I} - \frac{2}{3} \frac{p_\mu p_\nu}{m_I^2}, \quad (20)$$

or the spin  $\frac{5}{2}$  projection operator,

$$P_{\mu\nu,\mu'\nu'}^{\frac{5}{2}} = R_{\mu\nu,\mu'\nu'} - \frac{1}{5} P_{\mu\nu} P_{\mu'\nu'} - \frac{1}{5} (P_{\mu\rho} \gamma^\rho \gamma^\sigma R_{\sigma\nu,\mu'\nu'} + P_{\nu\rho} \gamma^\rho \gamma^\sigma R_{\sigma\mu,\mu'\nu'}), \quad (21)$$

with

$$R_{\mu\nu,\mu'\nu'} = \frac{1}{2} (P_{\mu\mu'} P_{\nu\nu'} + P_{\mu\nu'} P_{\nu\mu'}), \quad (22)$$

where

$$P_{\mu\nu} = g_{\mu\nu} - p_\mu p_\nu / m_I^2 \quad (23)$$

and  $m_I$  is the intermediate resonance mass.

In photoproduction  $p_u^2$  is generally small or negative, so the intermediate hyperon resonances in the  $u$  channel cannot decay. However, in the  $s$  channel,  $p_s^2$  is large enough that one or more decay channels may be open for the intermediate nucleon and  $\Delta$  resonances. Thus, widths must be included in the  $s$ -channel propagators, and these widths are both energy and momentum dependent. In earlier work involving the photoproduction of  $\Lambda$ 's, a dynamical model was developed for these widths [20], which I also employ here. In this model, the full decay width is decomposed into a number of partial widths for decay into various two- and three-body decay channels. In each such channel, the off-shell energy and momentum dependence is treated using an effective Lagrangian model with the required coupling strength adjusted to yield the empirical on-shell branching ratio for decay into that channel. For the two-body channels, this procedure yields straightforward expressions for the partial widths that depend on the spins and parities of both the resonances and the decay products.

Three-body decays are approximated as two-body decays with one stable decay product and one unstable decay product.

TABLE II.  $s$ -channel width data branching ratios.

Resonance	$c$ width (MeV)	Two-body channels			Three-body channels		
		$N\pi$	$N\eta$	$\Lambda K$	$N\sigma$	$\Delta(1232)\pi$	$N\rho$
$N(1440)$	350	0.60			0.15	0.25	
$N(1520)$	115	0.60				0.20	0.20
$N(1535)$	150	0.50	0.45				0.05
$N(1650)$	140	0.70	0.10	0.05		0.10	0.05
$N(1675)$	150	0.45				0.55	
$N(1680)$	130	0.68			0.12	0.10	0.10
$N(1700)$	150	0.12				0.68	0.20
$N(1710)$	100	0.12	0.20	0.10	0.18	0.25	0.15
$N(1720)$	250	0.10	0.05	0.05		0.40	0.40
$N(1860)$	200						
$N(1875)$	200	0.15	0.05		0.20	0.50	0.10
$N(1880)$	250						
$N(1900)$	250						
$N(2000)$	350						
$\Delta(1232)$	117	1.00					
$\Delta(1600)$	320	0.20				0.60	0.20
$\Delta(1620)$	140	0.25				0.55	0.20
$\Delta(1700)$	300	0.15				0.45	0.40
$\Delta(1905)$	330	0.12				0.70	0.18
$\Delta(1910)$	280	0.23		0.07			0.70
$\Delta(1920)$	260	0.20				0.80	
$\Delta(1930)$	360						

These are handled in the same fashion as the two-body decays except that the mass of the unstable decay product is assumed to be variable with a Breit-Wigner distribution. To obtain the corresponding width, it is necessary to integrate over this distribution. Details concerning the procedure, together with detailed expressions for the various widths so obtained, can be found in Ref. [19].

The dynamical width model is appropriate for resonances for which there are enough data to make reasonable estimates of the on-shell partial widths. This is the case for most of the well-established nucleon and  $\Delta$  resonances. For these resonances, I have updated the branching ratio information used in the previous  $\Lambda$  photoproduction fits to incorporate the data summarized in the most recent version of the particle data tables [24]. For the less well-established resonances, the branching ratio data are not sufficient to make use of the dynamical model. Hence, for these resonances, I employ the fixed on-shell width estimates given in the particle data tables.

Table II lists the on-shell width and branching ratio values that are employed in the present study. For the two-body branching ratios, the values used represent central values within the empirical ranges given in the tables. The three-body branching ratios are more uncertain. In Table II, any decay strength not allocated to one of the two-body channels is attributed to either the  $\pi\Delta$  or the  $\rho N$  decay channel using the particle data tables as a rough guide as to how to make the allocation. In practice, for several of the resonances, much of the three-body decay is attributed in the tables to an undifferentiated  $\pi\pi N$  channel, so that any allocation to  $\pi\Delta$  or  $\rho N$  channels is somewhat arbitrary. For resonances for which no branching ratio values appear in the table, in particular, for

the  $N(1880)$ ,  $N(1900)$ ,  $N(2000)$ , and  $\Delta(1930)$  resonances, the fixed resonance width prescription was employed. It should be noted again that the branching ratios in the table represent on-shell values. At energies below the threshold for a particular channel, the corresponding partial width is set equal to zero.

### III. FITTING PROCEDURE

The model described in the previous section for the reaction  $\gamma p \rightarrow K^+\Sigma^0$  was fit to cross-section and polarization data from a variety of sources. In particular, I fit CLAS data for the unpolarized differential cross section [25,26]; GRAAL data for  $\Sigma$ , the photon beam asymmetry [29]; CLAS data for  $P$ , the hyperon recoil asymmetry [26,27]; and CLAS data for the double-polarization observables,  $C_x$  and  $C_z$  [28]. The differential cross section is given in the center of mass (c.m.) by the expression

$$\frac{d\sigma}{d\Omega} = \frac{1}{(2\pi)^2} \frac{m_p m_\Sigma p_F}{4E_\gamma s} \frac{1}{4} \sum_{\text{spins}} |\langle F | \hat{T} | I \rangle|^2, \quad (24)$$

where  $p_F$  is outgoing three-momentum magnitude,  $s$  is the squared c.m. energy, and  $E_\gamma$  is the incident photon energy. The single-polarization observables are defined by the relations

$$\Sigma = \frac{d\sigma_\gamma^\perp - d\sigma_\gamma^\parallel}{d\sigma_\gamma^\perp + d\sigma_\gamma^\parallel}, \quad (25)$$

$$P = \frac{d\sigma_\Sigma^+ - d\sigma_\Sigma^-}{d\sigma_\Sigma^+ + d\sigma_\Sigma^-}, \quad (26)$$

TABLE III. Coupling strength products. The first column of numbers corresponds to fit 1 and the second column to fit 2, as described in the text.

Spin $\frac{1}{2}$ resonances			
$N(1440)$	$F_{N^*}$	-9.5359	-7.8671
$N(1535)$	$F_{N^*}$	2.1039	1.1034
$N(1650)$	$F_{N^*}$	0.2140	-0.0343
$N(1710)$	$F_{N^*}$	-0.2478	-0.0674
$N(1880)$	$F_{N^*}$	0.3145	1.0145
$\Delta(1620)$	$F_{\Delta}$	-1.2076	-0.7896
$\Delta(1910)$	$F_{\Delta}$	-0.2145	-1.4869
$\Lambda(1405)$	$F_{\Lambda^*}$	1.5253	2.2330
$\Lambda(1670)$	$F_{\Lambda^*}$	2.5702	0.0111
Spin $\frac{3}{2}$ resonances			
$N(1520)$	$G_{N^*}^1$	3.1726	2.0474
	$G_{N^*}^2$	2.5997	2.6298
$N(1700)$	$G_{N^*}^1$	5.5018	-2.8002
	$G_{N^*}^2$	4.2759	-4.1911
$N(1720)$	$G_{N^*}^1$	-0.0062	0.2572
	$G_{N^*}^2$	0.8729	-0.4442
$N(1875)$	$G_{N^*}^1$	-0.0687	-0.9594
	$G_{N^*}^2$	0.1179	-1.0823
$N(1900)$	$G_{N^*}^1$	-0.1417	0.1035
	$G_{N^*}^2$	-1.2793	0.0647
$\Delta(1232)$	$G_{\Delta}^1$	-0.2507	0.0870
	$G_{\Delta}^2$	-2.0684	-0.5610
$\Delta(1600)$	$G_{\Delta}^1$	0.4182	-0.9305
	$G_{\Delta}^2$	0.5768	3.1898
$\Delta(1700)$	$G_{\Delta}^1$	-7.3510	6.2298
	$G_{\Delta}^2$	-5.3411	8.9796
$\Delta(1920)$	$G_{\Delta}^1$	0.0735	-0.1417
	$G_{\Delta}^2$	1.4616	-0.0074
$\Lambda(1890)$	$G_{\Lambda^*}^1$	-8.3231	-7.3739
	$G_{\Lambda^*}^2$	7.7830	6.6918
$\Sigma(1385)$	$G_{\Sigma^*}^1$	2.3543	3.1159
	$G_{\Sigma^*}^2$	6.6994	-5.4446
$\Sigma(1940)$	$G_{\Sigma^*}^1$	5.9979	6.1471
	$G_{\Sigma^*}^2$	-9.0359	9.7442
Spin $\frac{5}{2}$ resonances			
$N(1675)$	$G_{N^*}^1$	0.0008	0.0080
	$G_{N^*}^2$	0.0418	0.0110
$N(1680)$	$G_{N^*}^1$	0.0426	-0.0993
	$G_{N^*}^2$	0.0191	-0.1965
$N(1860)$	$G_{N^*}^1$	-0.0888	-0.0608
	$G_{N^*}^2$	-0.1992	-0.0924
$N(2000)$	$G_{N^*}^1$	-0.0040	-0.0104
	$G_{N^*}^2$	-0.0522	-0.0129
$\Delta(1905)$	$G_{\Delta}^1$	0.0865	0.0974
	$G_{\Delta}^2$	0.2754	0.1695
$\Delta(1930)$	$G_{\Delta}^1$	-0.0009	-0.0002
	$G_{\Delta}^2$	-0.0066	-0.0022
$\Lambda(1820)$	$G_{\Lambda^*}^1$	1.6957	0.1079
	$G_{\Lambda^*}^2$	-0.3016	0.1811
$\Lambda(1830)$	$G_{\Lambda^*}^1$	-0.0056	0.0458
	$G_{\Lambda^*}^2$	6.1255	-0.6987

TABLE III. (Continued.)

Spin $\frac{5}{2}$ resonances			
$\Lambda(2110)$	$G_{\Lambda^*}^1$	2.2253	-0.1345
	$G_{\Lambda^*}^2$	-1.8388	-0.2581
$\Sigma(1775)$	$G_{\Sigma^*}^1$	-0.0675	-0.0567
	$G_{\Sigma^*}^2$	-5.4884	0.6461
$\Sigma(1915)$	$G_{\Sigma^*}^1$	-3.6871	0.0585
	$G_{\Sigma^*}^2$	1.4414	0.1698
Kaon resonances			
$K(892)$	$G_{K^*}^V$	10.2218	8.6461
	$G_{K^*}^T$	4.3609	2.1909
$K(1270)$	$G_{K^*}^V$	-2.1659	11.9499
	$G_{K^*}^T$	18.7692	3.7975

where the superscripts  $\perp$  and  $\parallel$  refer to photon polarizations perpendicular and parallel to the scattering plane and the superscripts  $+$  and  $-$  refer to  $\Sigma$  spin projections above and below the scattering plane. The double-polarization variables are defined for circularly polarized photons with positive

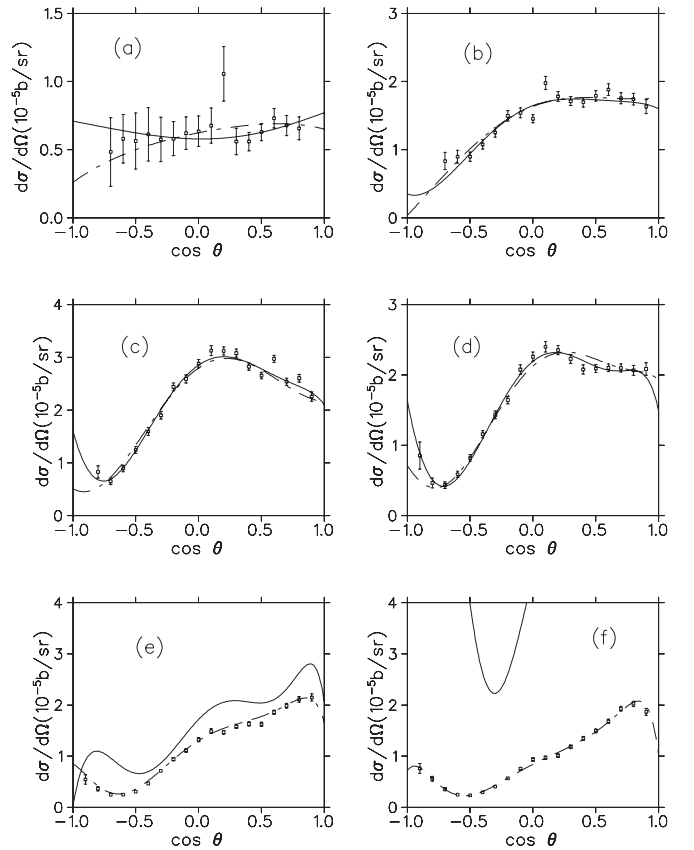


FIG. 2. Differential cross section vs  $\cos\theta_{c.m.}$  for (a)  $E_{c.m.} = 1.715$  GeV, (b)  $E_{c.m.} = 1.795$  GeV, (c)  $E_{c.m.} = 1.875$  GeV, (d)  $E_{c.m.} = 1.945$  GeV, (e)  $E_{c.m.} = 2.025$  GeV, and (f)  $E_{c.m.} = 2.105$  GeV. The solid curves were obtained with fit 1 and the dot-dashed curves with fit 2, as described in the text. Data are from Refs. [25,26].

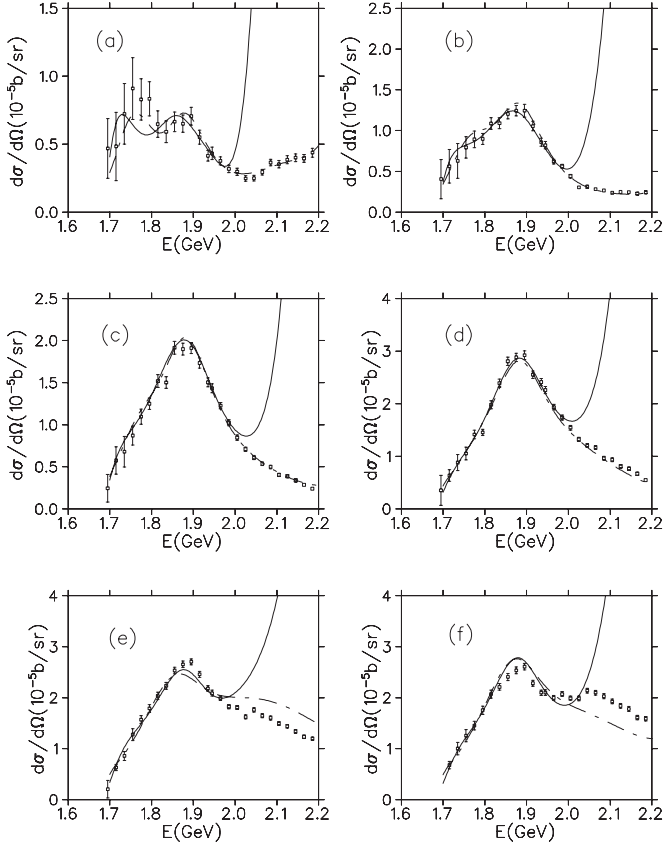


FIG. 3. Differential cross section vs  $E_{c.m.}$  for (a)  $\cos \theta_{c.m.} = -0.7$ , (b)  $\cos \theta_{c.m.} = -0.5$ , (c)  $\cos \theta_{c.m.} = -0.3$ , (d)  $\cos \theta_{c.m.} = 0$ , (e)  $\cos \theta_{c.m.} = 0.5$ , and (f)  $\cos \theta_{c.m.} = 0.7$ . The solid curves were obtained with fit 1 and the dot-dashed curves with fit 2, as described in the text. Data are from Refs. [25,26].

helicity by the relation

$$C_i = \frac{d\sigma_{\Sigma^+} - d\sigma_{\Sigma^-}}{d\sigma_{\Sigma^+} + d\sigma_{\Sigma^-}}, \quad (27)$$

where now the superscripts  $+$  and  $-$  refer to  $\Sigma$  spin projections along and opposite to either the  $z$  ( $i = z$ ) or  $x$  ( $i = x$ ) axes.

The fits were carried out by minimizing the  $\chi^2$  per degree of freedom defined by the relation

$$\frac{\chi^2}{\nu} = \sum \frac{(Y_{\text{calc}} - Y_{\text{exp}})^2}{\sigma^2}, \quad (28)$$

where the sum is over the data points employed in the fit,  $Y_{\text{calc}}$  and  $Y_{\text{exp}}$  are calculated and measured values for the observable corresponding to a particular data point, and  $\sigma^2$  is the squared uncertainty in  $Y_{\text{exp}}$ . The number of degrees of freedom in the fit is given by  $\nu = N_{\text{data}} - N_{\text{par}}$ , where  $N_{\text{data}}$  is the number of data points and  $N_{\text{par}}$  the number of fit parameters. For some of the energies considered, the empirical values for  $C_x$  or  $C_z$  lie outside the mathematically allowed ranges for these parameters, i.e., have magnitudes that exceed unity. Because such values cannot be fit in any theoretical model, I have simply excluded them from the fit data set.

The fit parameters consist of the products of the coupling strengths at the electromagnetic and strong interaction vertices

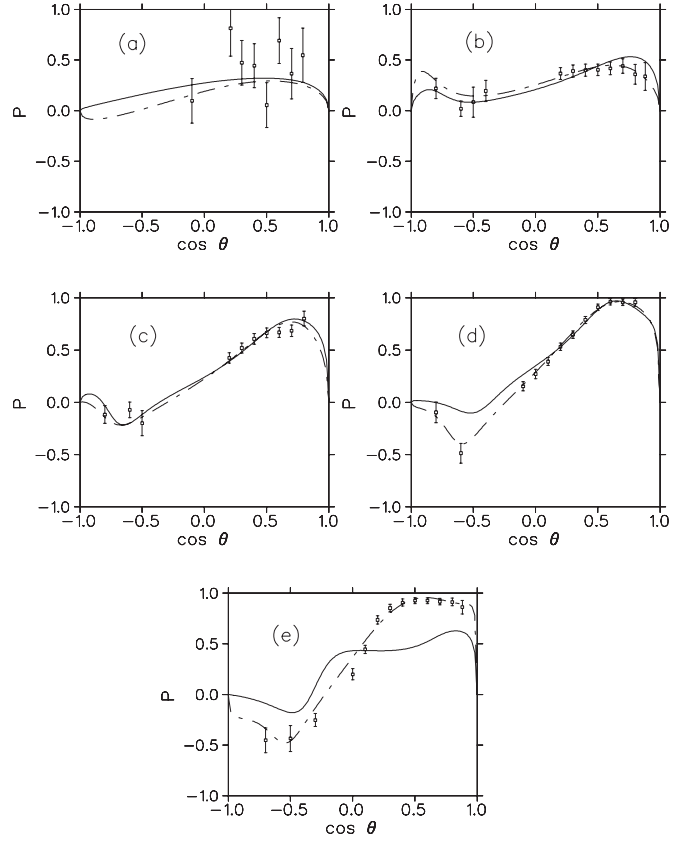


FIG. 4. Hyperon recoil asymmetry vs  $\cos \theta_{c.m.}$  for (a)  $E_{c.m.} = 1.729$  GeV, (b)  $E_{c.m.} = 1.844$  GeV, (c)  $E_{c.m.} = 1.933$  GeV, (d)  $E_{c.m.} = 2.024$  GeV, and (e)  $E_{c.m.} = 2.111$  GeV. The solid curves were obtained with fit 1 and the dot-dashed curves with fit 2, as described in the text. Data are from Refs. [26,27].

for all resonances incorporated in the fit. These are defined by the relations

$$\begin{aligned} F_{N^*} &= e\kappa_{pN^*} g_{\Sigma KN^*}, \\ F_{\Delta} &= e\kappa_{p\Delta} g_{\Sigma K\Delta}, \\ F_Y &= e\kappa_{\Sigma Y} g_{YKp}, \end{aligned} \quad (29)$$

for spin  $\frac{1}{2}$  baryon resonances; by

$$\begin{aligned} G_{N^*}^1 &= g_1^{pN^*} g_{\Sigma KN^*}, \\ G_{N^*}^2 &= g_2^{pN^*} g_{\Sigma KN^*}, \\ G_{\Delta}^1 &= g_1^{p\Delta} g_{\Sigma K\Delta}, \\ G_{\Delta}^2 &= g_2^{p\Delta} g_{\Sigma K\Delta}, \\ G_Y^1 &= g_1^{\Sigma Y} g_{YKp}, \\ G_Y^2 &= g_2^{\Sigma Y} g_{YKp}, \end{aligned} \quad (30)$$

for spin  $\frac{3}{2}$  and spin  $\frac{5}{2}$  baryon resonances; and by

$$\begin{aligned} G_{K^*}^V &= g_{\gamma KK^*} g_{\Sigma K^* p}^V, \\ G_{K^*}^T &= g_{\gamma KK^*} g_{\Sigma K^* p}^T, \end{aligned} \quad (31)$$

for the kaon resonances.

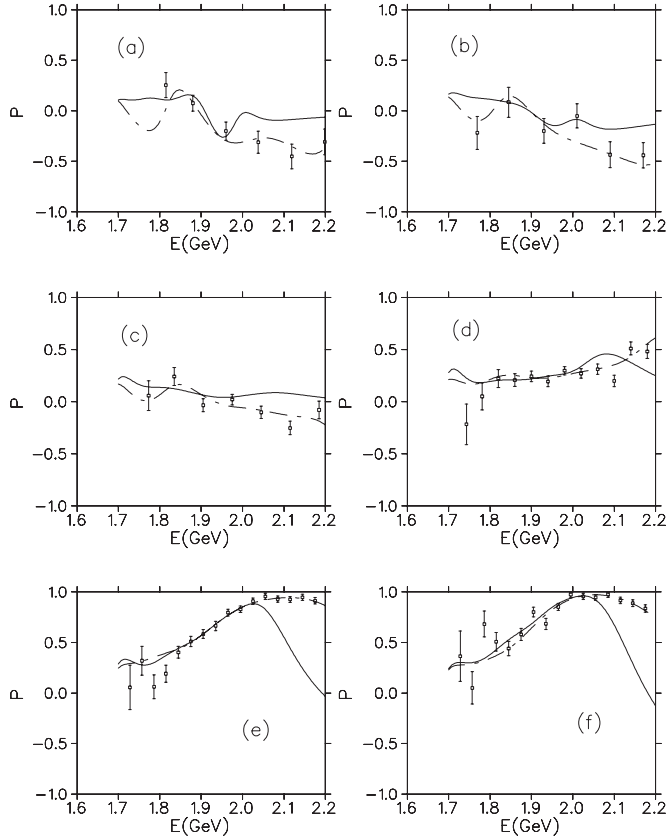


FIG. 5. Hyperon recoil asymmetry vs  $E_{c.m.}$  for (a)  $\cos\theta_{c.m.} = -0.7$ , (b)  $\cos\theta_{c.m.} = -0.5$ , (c)  $\cos\theta_{c.m.} = -0.3$ , (d)  $\cos\theta_{c.m.} = 0$ , (e)  $\cos\theta_{c.m.} = 0.5$ , and (f)  $\cos\theta_{c.m.} = 0.7$ . The solid curves were obtained with fit 1 and the dot-dashed curves with fit 2, as described in the text. Data are from Refs. [26,27].

For the Born term couplings, I employ fixed values determined through the use of empirical data and symmetry relations. In particular, for the electromagnetic couplings, the particle data tables [24] yield the values  $\kappa_p = 1.79$ ,  $\mu_{\Sigma^+} = 2.46\mu_N$ ,  $\mu_{\Sigma^-} = -1.16\mu_N$ , and  $\mu_T = 1.61\mu_N$ , where  $\mu_N$  is the nucleon magneton and the value given for the  $\Lambda\Sigma^0$  transition magnetic moment  $\mu_T$  is an absolute value. Because there is no empirical value for the magnetic moment of the neutral  $\Sigma$ , I use the simple quark model relation,  $\mu_{\Sigma^0} = \frac{1}{2}(\mu_{\Sigma^+} + \mu_{\Sigma^-})$ , which yields the value  $\mu_{\Sigma^0} = 0.650\mu_N$ . For the transition magnetic moment, only the absolute value has been determined empirically. In the previous  $\Lambda$  photoproduction fits, a positive value was adopted for this magnetic moment. However, the quark model predicts a negative value, so I have employed a negative value for  $\mu_T$  in the present study. The corresponding values for the  $\kappa$ 's appearing in Eq. (13) are

$$\begin{aligned}\kappa_{\Sigma^0} &= \frac{m_{\Sigma^0}}{m_p} \frac{\mu_{\Sigma^0}}{\mu_N} = 0.825, \\ \kappa_T &= \frac{m_{\Sigma^0}}{m_p} \frac{\mu_T}{\mu_N} = -2.04.\end{aligned}\quad (32)$$

For the strong interaction couplings, I begin with the value for the  $\Lambda Kp$  coupling that was used in the previous  $\Lambda$  electroproduction studies [22], namely,  $g_{\Lambda Kp} = -6.537$ .

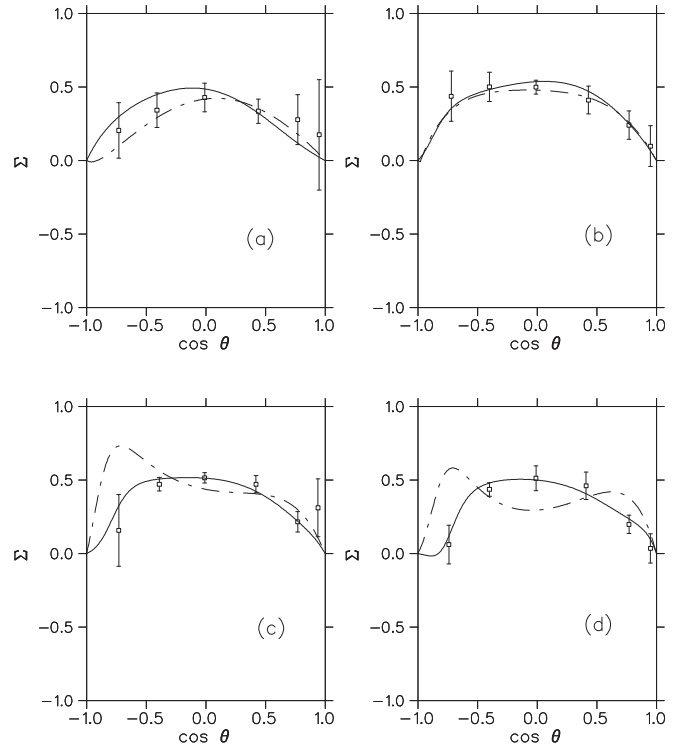


FIG. 6. Photon beam asymmetry vs  $\cos\theta_{c.m.}$  for (a)  $E_{c.m.} = 1.755$  GeV, (b)  $E_{c.m.} = 1.808$  GeV, (c)  $E_{c.m.} = 1.858$  GeV, and (d)  $E_{c.m.} = 1.906$  GeV. The solid curves were obtained with fit 1, and the dot-dashed curves with fit 2, as described in the text. Data are from Ref. [29].

From this value, a value for the  $\Sigma^0 Kp$  coupling strength can be extracted from the SU(3) symmetry relation

$$g_{\Sigma Kp} = \frac{1 - 2\alpha}{\sqrt{3}(1 - \frac{2}{3}\alpha)} g_{\Lambda Kp}. \quad (33)$$

Using  $\alpha = 0.625$  yields  $g_{\Sigma Kp} = 1.615$ , so that for the Born coupling strength products I obtain

$$\begin{aligned}F_{Cp} &= e g_{\Sigma Kp} = 0.489, \\ F_p &= e \kappa_p g_{\Sigma Kp} = 0.876, \\ F_{\Sigma} &= e \kappa_{\Sigma^0} g_{\Sigma Kp} = 0.403, \\ F_{\Lambda} &= e \kappa_T g_{\Lambda Kp} = 4.04, \\ F_K &= F_{Cp} = 0.489,\end{aligned}\quad (34)$$

where  $F_{Cp}$  is the coupling product associated with the proton charge term and the dimensionless value  $e = 0.3029$  has been employed.

#### IV. RESULTS AND DISCUSSION

The coupling constant products associated with the two fits are listed in Table III. The first column of numbers corresponds to a fit of the data from threshold up to a c.m. energy of 2.0 GeV (fit 1), while the second column corresponds to a fit from threshold up to 2.2 GeV (fit 2). Although the maximum energies associated with the two fits differ by only 0.2 GeV, the

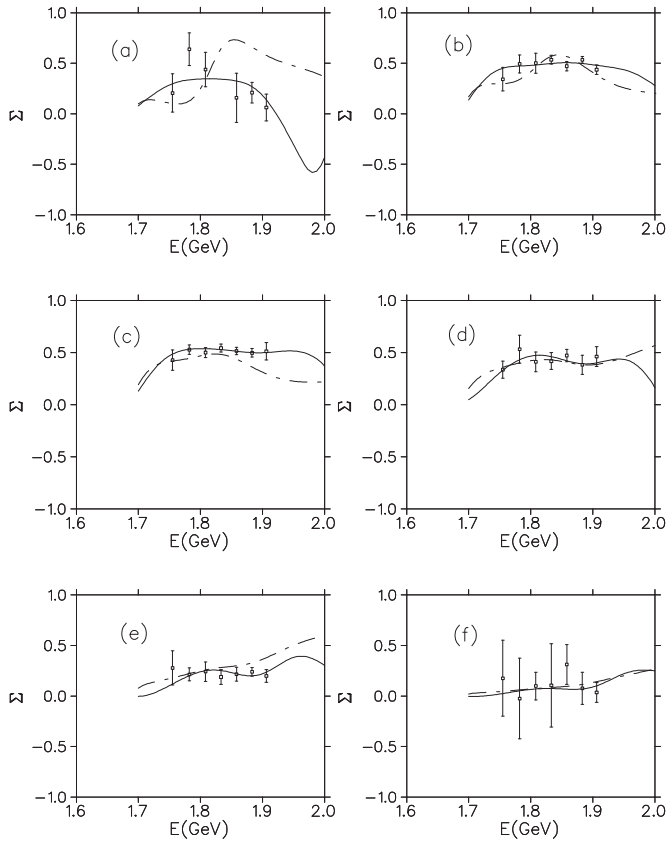


FIG. 7. Photon beam asymmetry vs  $E_{c.m.}$  for (a)  $\cos\theta_{c.m.} = -0.73$ , (b)  $\cos\theta_{c.m.} = -0.4$ , (c)  $\cos\theta_{c.m.} = 0$ , (d)  $\cos\theta_{c.m.} = 0.426$ , (e)  $\cos\theta_{c.m.} = 0.77$ , and (f)  $\cos\theta_{c.m.} = 0.947$ . The solid curves were obtained with fit 1 and the dot-dashed curves with fit 2, as described in the text. Data are from Ref. [29].

$\chi^2$  values obtained with the two fits are significantly different. The fit with the lower energy cutoff has a  $\chi^2$  value of about 1.4; the value 2.2 obtained for the  $\chi^2$  with the higher energy cutoff is substantially higher. As Table III reveals, the couplings generated in the two fits are similar for some parameters, but rather different for others.

The fit qualities are illustrated in Figs. 2–10, where in each figure the solid curves were obtained with fit 1 and the dot-dashed curves with fit 2. In the first of these figures, Fig. 2, the angular distribution of the unpolarized cross section is displayed for several values of the total c.m. energy. Note that the cross sections in both this figure and Fig. 3 have been multiplied by a factor of 10 so as to have units of  $10^{-5}$  b/sr. At the four lower energies, the two fits yield equally good representations of the data, although at the lowest energy, the angular distributions resulting from the two fits are qualitatively different. At energies exceeding the cutoff energy of fit 1 (bottom two panels), only fit 2 yields a good representation of the data.

The failure of fit 1 at energies exceeding its cutoff energy is shown more dramatically in Fig. 3, where the energy dependence of the unpolarized cross section is displayed for several values of the kaon c.m. scattering angle. Here it can be seen that each fit yields a fairly good representation of the

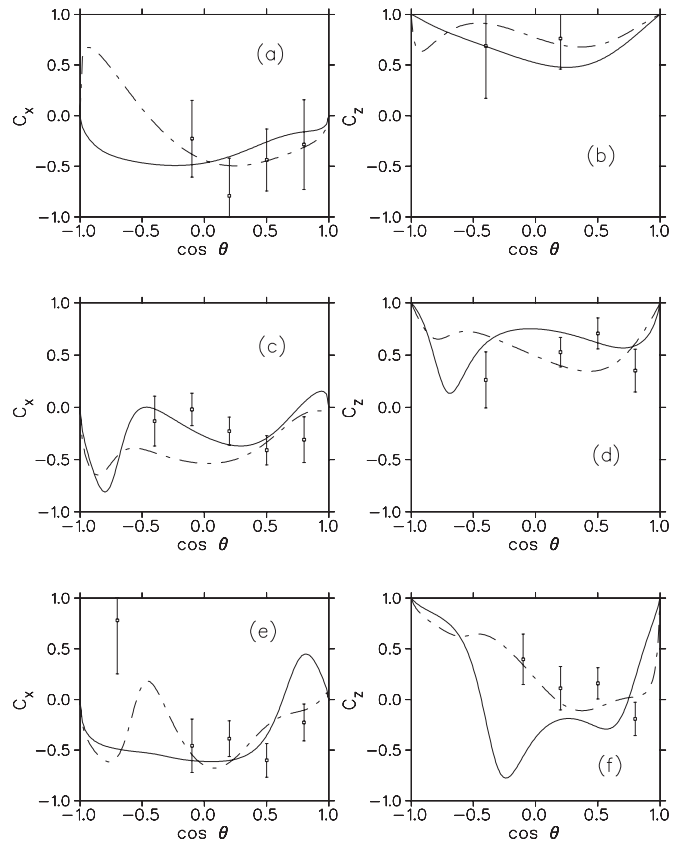


FIG. 8. Double-polarization parameter  $C_X$  vs  $\cos\theta_{c.m.}$  for (a)  $E_{c.m.} = 1.787$  GeV, (c)  $E_{c.m.} = 1.939$  GeV, and (e)  $E_{c.m.} = 2.126$  GeV; and double-polarization parameter  $C_Z$  vs  $\cos\theta_{c.m.}$  for (b)  $E_{c.m.} = 1.787$  GeV, (d)  $E_{c.m.} = 1.939$  GeV, and (f)  $E_{c.m.} = 2.126$  GeV. The solid curves were obtained with fit 1 and the dot-dashed curves with fit 2, as described in the text. Data are from Ref. [28].

data up to the cutoff energy for that fit. While fit 1 departs significantly from the data at energies above 2.0 GeV, fit 2 remains fairly close to the data up to 2.2 GeV, although even fit 2 does not reproduce the data well at forward angles for energies above 2.0 GeV. The fact that the fit 1 cross section increases rapidly at energies above the cutoff for that fit suggests that the correct cross-section normalization is achieved in the fits through rather delicate cancellations among the many contributions.

Figures 4 and 5 display the angular and energy distributions of the hyperon recoil asymmetry. As for the unpolarized cross section, both fits yield good representations of the angular distributions at energies below 2.0 GeV. At an energy of 2.024 GeV [Fig. 4(d)], fit 1 already shows a discrepancy with the data at backward angles and fails completely at 2.111 GeV, while fit 2 reproduces the empirical angular distributions quite well at both energies. The energy distributions reinforce these conclusions. Fit 1 reproduces the data only up to 2.0 GeV, while fit 2 accounts for the data up to 2.2 GeV.

Results for the photon beam asymmetry are displayed in Figs. 6 and 7. The GRAAL data for this parameter do not extend beyond 2.0 GeV, so in principle, both fits should give

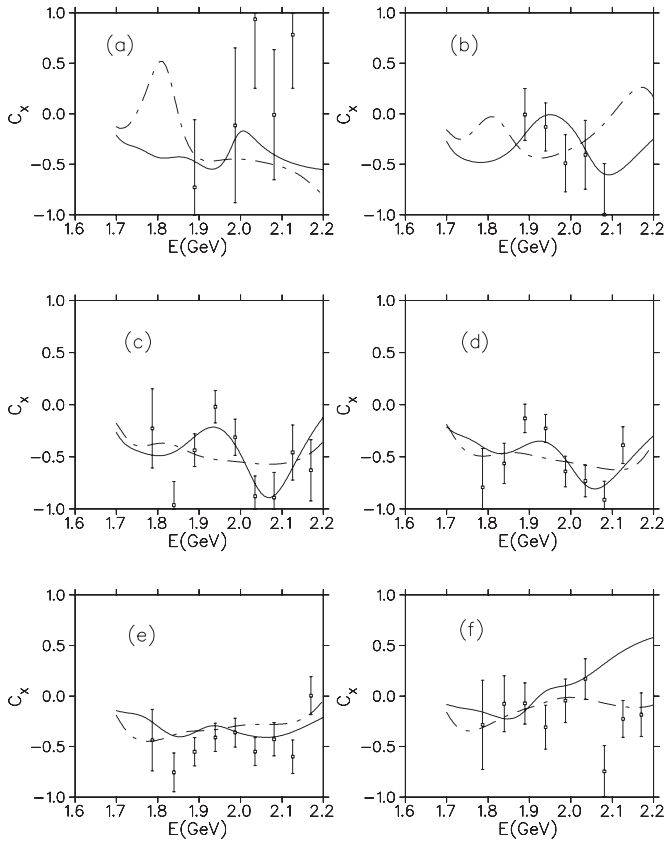


FIG. 9. Double-polarization parameter  $C_X$  vs  $E_{c.m.}$  for (a)  $\cos\theta_{c.m.} = -0.7$ , (b)  $\cos\theta_{c.m.} = -0.4$ , (c)  $\cos\theta_{c.m.} = -0.1$ , (d)  $\cos\theta_{c.m.} = 0.2$ , (e)  $\cos\theta_{c.m.} = 0.5$ , and (f)  $\cos\theta_{c.m.} = 0.8$ . The solid curves were obtained with fit 1 and the dot-dashed curves with fit 2, as described in the text. Data are from Ref. [28].

good representations of the data. In practice, fit 1 does a better job, which probably reflects the lower  $\chi^2$  value associated with that fit. At the two higher energies in Fig. 6 (bottom two panels), the angular distributions obtained with fit 2 contain a backward peak that is not present in either the data or the fit 1 results. This discrepancy between the fit 2 results and the data at backwards angles is also seen in the energy distributions obtained for  $\cos\theta_{c.m.} = -0.73$  [Fig. 7(a)], where fit 2 completely misses the three data points above 1.85 GeV.

The last three figures, Figs. 8, 9, and 10, display results for the double-polarization parameters  $C_x$  and  $C_z$ . Note that the first of these figures (Fig. 8) exhibits angular distributions for both parameters ( $C_x$  in the left-hand panels,  $C_z$  in the right-hand panels). The quality of the data for these parameters is limited, but it appears that the fit 1 angular distributions are somewhat superior at the intermediate energy (middle panels), while fit 2 is better at the higher energy, particularly for  $C_z$ . The energy distribution results for  $C_x$  (Fig. 9) are not really conclusive; neither fit is obviously superior to the other. The  $C_z$  energy distribution results (Fig. 10), however, clearly exhibit the superiority of fit 2 at energies above 2.0 GeV.

In summary, two new fits have been obtained for the reaction  $\gamma p \rightarrow K^+ \Sigma^0$  using a tree-level effective Lagrangian

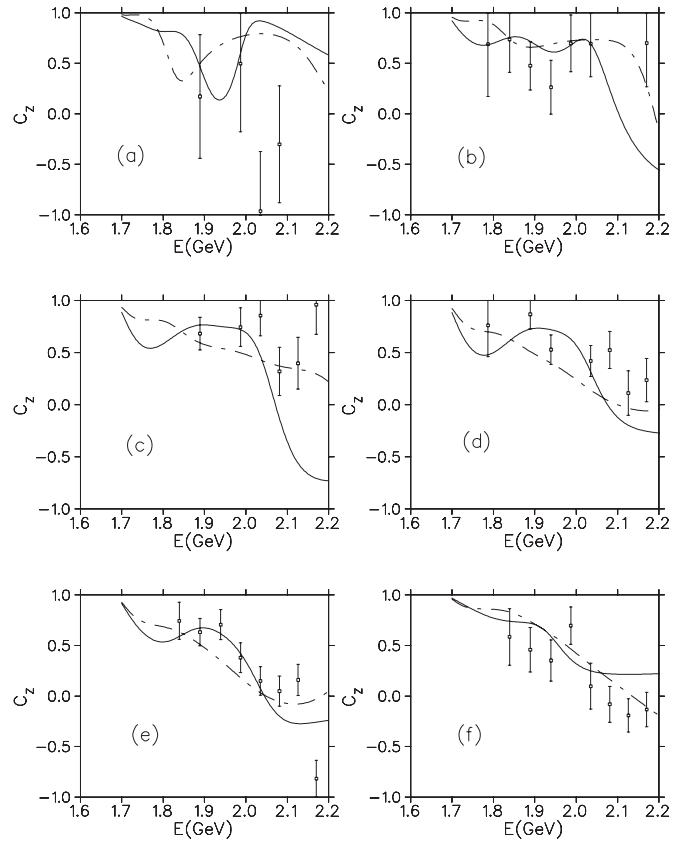


FIG. 10. Double-polarization parameter  $C_Z$  vs  $E_{c.m.}$  for (a)  $\cos\theta_{c.m.} = -0.7$ , (b)  $\cos\theta_{c.m.} = -0.4$ , (c)  $\cos\theta_{c.m.} = -0.1$ , (d)  $\cos\theta_{c.m.} = 0.2$ , (e)  $\cos\theta_{c.m.} = 0.5$ , and (f)  $\cos\theta_{c.m.} = 0.8$ . The solid curves were obtained with fit 1 and the dot-dashed curves with fit 2, as described in the text. Data are from Ref. [28].

model similar to that employed previously to study the photoproduction of  $\Lambda$ 's. The model incorporates most of the well-established nucleon and  $\Delta$  resonances in the  $s$  channel, as well as several less well-established nucleon and  $\Delta$  resonances of higher energy. It also includes a variety of hyperon resonances in the  $u$  channel and two kaon resonances in the  $t$  channel. The first of the two fits is of higher quality and incorporates data from threshold up to a maximum c.m. energy of 2.0 GeV. The second fit extends the fit energy range up to 2.2 GeV, but at the expense of a higher  $\chi^2$  per degree of freedom. Both fits give good accounts of a variety of CEBAF and GRAAL data over their respective energy ranges.

The fits described here suffer the usual limitations of fits based on tree-level effective Lagrangian models. Because the parameters associated with the  $s$ -,  $u$ -, and  $t$ -channel resonances are obtained independently of one another, the fits are not explicitly unitary. Moreover, the fits do not take account of possible coupling with other outgoing channels, such as the  $K^0 \Sigma^+$  channel. Finally, because the success of the fit depends on the delicate balancing of a fairly large number of parameters, it cannot be reliably used outside the fitted energy range.

Besides photoproduction data, there exist data for the electroproduction of  $\Sigma^0$ 's from the proton [30]. The fits

described in this work could be extended to electroproduction through the inclusion of electromagnetic form factors. Work in this direction is currently in progress. There also exist data

for the electroproduction of  $\Sigma^0$ 's from the deuteron and  ${}^3\text{He}$  [31]; the consideration of these reactions represents another direction in which the present work could be extended.

- 
- [1] H. Thom, E. Gabathuler, D. Jones, B. D. McDaniel, and W. M. Woodward, *Phys. Rev. Lett.* **11**, 433 (1963); M. Grilli, L. Mezzetti, M. Nigro, and E. Schiavuta, *Nuovo Cimento* **38**, 1467 (1965); H. Thom, *Phys. Rev.* **151**, 1322 (1966); D. E. Groom and J. H. Marshall, *ibid.* **159**, 1213 (1967); T. Fujii *et al.*, *Phys. Rev. D* **2**, 439 (1970).
- [2] F. M. Renard and Y. Renard, *Nucl. Phys. B* **1**, 389 (1967); *Phys. Lett. B* **24**, 159 (1967); *Nucl. Phys. B* **25**, 490 (1971); Y. Renard, *ibid.* **40**, 499 (1972).
- [3] R. A. Adelseck, C. Bennhold, and L. E. Wright, *Phys. Rev. C* **32**, 1681 (1985); R. A. Adelseck and L. E. Wright, *ibid.* **38**, 1965 (1988); R. A. Adelseck and B. Saghai, *ibid.* **42**, 108 (1990).
- [4] Robert A. Williams, C.-R. Ji, and S. R. Cotanch, *Phys. Rev. C* **46**, 1617 (1992).
- [5] T. Mart, C. Bennhold, and C. E. Hyde-Wright, *Phys. Rev. C* **51**, R1074 (1995); H. Haberzettl, C. Bennhold, T. Mart, and T. Feuster, *ibid.* **58**, R40 (1998); T. Mart and C. Bennhold, *Nucl. Phys. A* **639**, 237c (1998); H. Haberzettl, C. Bennhold, and T. Mart, *ibid.* **684**, 475 (2001).
- [6] M. K. Cheoun, B. S. Han, B. G. Yu, and I.-T. Cheon, *Phys. Rev. C* **54**, 1811 (1996); B. S. Han, M. K. Cheoun, K. S. Kim, and I.-T. Cheon, *Nucl. Phys. A* **691**, 713 (2001).
- [7] T. Mizutani, C. Fayard, G.-H. Lamot, and B. Saghai, *Phys. Rev. C* **58**, 75 (1998).
- [8] S. S. Hsiao, D. H. Lu, and S. N. Yang, *Phys. Rev. C* **61**, 068201 (2000).
- [9] W. T. Chiang, F. Tabakin, T.-S. H. Lee, and B. Saghai, *Phys. Lett. B* **517**, 101 (2001).
- [10] S. Janssen, J. Ryckebusch, W. V. Nespén, D. Debruyne, and T. Van Cauteren, *Eur. Phys. J. A* **11**, 105 (2001); S. Janssen, J. Ryckebusch, D. Debruyne, and T. Van Cauteren, *Phys. Rev. C* **65**, 015201 (2001); **66**, 035202 (2002); S. Janssen, J. Ryckebusch, and T. Van Cauteren, *ibid.* **67**, 052201(R) (2003); S. Janssen, D. G. Ireland, and J. Ryckebusch, *Phys. Lett. B* **562**, 51 (2003).
- [11] Oren V. Maxwell, *Phys. Rev. C* **70**, 044612 (2004).
- [12] Oren V. Maxwell, *Phys. Rev. C* **76**, 014621 (2007).
- [13] Z. Li, *Phys. Rev. C* **52**, 1648 (1995); Z. Li, M. Wei-Hsing, and Z. Lin, *ibid.* **54**, R2171 (1996).
- [14] J. C. David, C. Fayard, G. H. Lamot, and B. Saghai, *Phys. Rev. C* **53**, 2613 (1996).
- [15] A. Usov and O. Scholten, *Phys. Rev. C* **72**, 025205 (2005).
- [16] A. V. Sarantsev, V. A. Nikonov, A. V. Anisovich, E. Klempt, and U. Thoma, *Eur. Phys. J. A* **25**, 441 (2005); A. V. Anisovich, R. Beck, E. Klempt, V. A. Nikonov, A. V. Sarantsev, and U. Thoma, *ibid.* **48**, 88 (2012).
- [17] Xu Cao, V. Shklyar, and H. Lenske, *Phys. Rev. C* **88**, 055204 (2013).
- [18] T. Mart, *Phys. Rev. C* **90**, 065202 (2014).
- [19] A. de la Puente, O. V. Maxwell, and B. A. Raue, *Phys. Rev. C* **80**, 065205 (2009).
- [20] O. V. Maxwell, *Phys. Rev. C* **69**, 034605 (2004).
- [21] O. V. Maxwell, *Phys. Rev. C* **72**, 034601 (2005).
- [22] O. V. Maxwell, *Phys. Rev. C* **85**, 034611 (2012).
- [23] O. V. Maxwell, *Phys. Rev. C* **86**, 064612 (2012); **89**, 024001 (2014); **90**, 034605 (2014).
- [24] K. A. Olive *et al.* (Particle Data Group), *Chin. Phys. C* **38**, 090001 (2014).
- [25] R. Bradford *et al.*, *Phys. Rev. C* **73**, 035202 (2006).
- [26] B. Dey *et al.*, *Phys. Rev. C* **82**, 025202 (2010).
- [27] J. W. C. McNabb *et al.*, *Phys. Rev. C* **69**, 042201 (2004).
- [28] R. Bradford *et al.*, *Phys. Rev. C* **75**, 035205 (2007).
- [29] A. Lleres *et al.*, *Eur. Phys. J. A* **31**, 79 (2007).
- [30] A. Ambrozewicz *et al.*, *Phys. Rev. C* **75**, 045203 (2007); D. S. Carman *et al.*, *ibid.* **79**, 065205 (2009); **87**, 025204 (2013).
- [31] D. Abbott *et al.*, *Nucl. Phys. A* **639**, 197c (1998); J. Reinhold *et al.*, *ibid.* **684**, 470 (2001); B. Zeidman *et al.*, *ibid.* **691**, 37 (2001); F. Dohrmann *et al.*, *Phys. Rev. C* **76**, 054004 (2007).